THE JOURNAL OF PHYSICAL CHEMISTRY C

Article

Chemically Tunable Properties of Graphene Covered Simultaneously with Hydroxyl and Epoxy Groups

Ivan Guilhon Mitoso Rocha, Friedhelm Bechstedt, Silvana Botti, Marcelo Marques, and Lara Kühl Teles

J. Phys. Chem. C, **Just Accepted Manuscript** • DOI: 10.1021/acs.jpcc.7b09513 • Publication Date (Web): 17 Nov 2017

Chemically Tunable Properties of Graphene Covered Simultaneously with Hydroxyl and Epoxy Groups

I. Guilhon,[†,‡] F. Bechstedt,[‡] Silvana Botti,[‡] M. Marques,[†] and L. K. Teles[*,†]

†*Grupo de Materiais Semicondutores e Nanotecnologia, Instituto Tecnológico de Aeronáutica, DCTA, 12228-900 São José dos Campos, Brazil*

‡*Institut für Festkörpertheorie und -optik, Friedrich-Schiller-Universität and ETSF, Max-Wien-Platz 1, D-07743 Jena, Germany*

E-mail: lkteles@ita.br

Abstract

We investigate the chemically tunable properties of understoichiometric graphene oxide as a function of the growth temperature and the amount of hydroxyl and epoxy groups adsorbed on graphene. The structural disorder is modeled within a statistical approach based on a cluster expansion. A set of 308 cluster symmetry classes is investigated with *ab initio* calculations based on density functional theory. A complete scenario of energetics and phase stability is developed, yielding insight into the structure and electronic properties of graphene oxide. Our results show that the tendency to agglomeration of oxygen-containing groups is independent of their relative proportion, and indicate the favorable formation of a unique oxygen-rich phase with both groups. Structural and electronic properties are predicted for the whole range of chemical compositions. The optical properties of oxygen-rich phases are also discussed in detail for different growth conditions.

Introduction

Graphene is a material with exceptional mechanical, electronic and thermal properties.[1,2] The discovery of graphene and the emergence of its unique physical properties has attracted great interest both from academia and industry, also in view of the possibility of miniaturization of devices. However, the fact that its band structure exhibits no energy gap limits its electronic and optical applications.

Chemical functionalization by oxygen and hydrogen has been proposed to overcome these limitations. Fully oxidized graphene, called graphene oxide (or GO), or hydrogenated graphene, known as graphane, display open energy gaps and exhibit significantly different electronic and optical properties with respect to their parent graphene.[3–7] This new class of two-dimensional (2D) graphene-based materials is therefore actively studied for applications.

Indeed, GO is a strong candidate for a 2D platform with tunable electronic properties compatible to graphene technology. GO has already been employed in 2D sensor devices,[8,9]

electronics,[10–12] optoelectronics[4,12] and supercapacitors.[13] The first GO samples were chemically exfoliated about 150 years ago by Brodie[14] from graphite oxide. However, due to its amorphous nature, the details of its atomic structure are still under debate.[3,5] Different models have been proposed to study the atomic structure of GO and explain its properties.[6,15–18] Recent NMR measurements have shed light on the chemical bonding of hydroxyl (−OH) and epoxy (−O−) groups on graphene sheets. The experimental findings indicate that the two chemical groups tend to be adsorbed close to each other.[19] GO is usually synthesized from graphite powder using oxidant solutions and subsequent exfoliation.[5] The wet chemical treatment of graphene and the exposure to oxygen plasma are also successful ways to obtain GO samples.[20]

Graphene oxide sheets samples may still exhibit sp^2 carbons due to an incomplete oxidation process ($y+z<1$). We refer to these systems as understoichiometric GO, which can also be obtained by chemical reduction of fully-oxidized GO.[21] The understoichiometric oxides allow tuning their properties between those of GO and graphene. This interesting concept of chemical tuning properties has been applied to many 2D alloys in experimental[22–27] and theoretical works.[28–31] Analogously, it is possible to partially functionalize sheets, as demonstrated for the adsorption of hydrogen,[32,33] halogen[34,35] and oxygen-containing groups on graphene sheets.[4,36–38]

In a previous work,[39] we have investigated the tunable properties of understoichiometric GO, considering the effect of a separate adsorption of −OH or −O− on graphene. These two cases correspond, respectively, to wet and dry environmental growth condition limits. However, it is known that in practice more than one adsorbed group, e.g. −OH and −O−, may coexist below or above the graphene basal plane of a understoichiometric GO.[36–38] The effect of the coexistence of different oxygen-containing groups on the thermodynamic stability, atomic positions and resulting electronic and optical properties are less studied and, therefore, not yet completely understood.

In this work, we study the simultaneous adsorption of hydroxyl and epoxy groups on

graphene in a more realistic scenario. They can be interpretated as chemical variations between pure graphene, fully oxidized graphene with only −OH groups, and fully oxidized graphene with only −O− groups. The theoretical treatment of the simultaneous adsorption by hydroxyl and epoxy groups requires the development of a statistical approach for functionalized graphene sheets in great similarity to a ternary alloy. Therefore, we generalize the method based on cluster expansion, that we had proposed for in Ref.[39] for single adsorbed group species, to the case of simultaneous decoration of a graphene sheet with two different oxygen-containing groups. We focus on unambiguous new features of GO energetics, for instance the increase of thermodynamic stability for low-energy fully oxidized graphene when both both hydroxyl and epoxy groups are simultaneously adsorbed. The increased chemical flexibility gives rise to a larger range of energy gap, and hence a greater potential for band gap engineering. Ordered geometries may indicate that the oxygen-containing groups agglomerate in a unique oxygen-rich phase.

The paper is organized as follows. In Methods section we present the statistical approach that we use to describe the simultaneous incomplete oxidation with two oxidant groups. Computational details are also included. A full picture of the properties of GO as a function of its chemical composition is given in Results and discussion section. The thermodynamic analysis of GO demonstrates that the previously reported strong tendency to phase separation into oxygen-poor and -rich domains[39] is robust against variations of the relative abundance of the hydroxyl and epoxy groups. Structural, electronic and optical properties for typical growth temperatures are calculated and explained in terms of the most stable local atomic arrangements. The theoretical results are compared with experimental data whenever it is possible. Finally, the main results and conclusions are organized in the Summary section.

Methods

Statistical approach

The effects of bonding and disorder on the distribution of oxygen-containing groups adsorbed on a graphene layer are here studied using a cluster expansion approach, known as Generalized Quasi Chemical Approximation (GQCA).[40] This formalism has been successfully applied to several 2D and 3D alloys,[28,29,41,42] and, more recently, generalized to functionalized 2D sheets.[39] The disordered system is decomposed into clusters with n carbon atoms, which are considered statistically and energetically independent from each other.[40] This approximation is more realistic and accurate when the clusters become larger. However, the number of atomic configurations that must be considered dramatically increases with the supercell size. As a consequence, the cluster size must be chosen as a compromise between precision and the number of configurations to be calculated.

Here, we need to generalize the method to the case of simultaneous adsorption of $-$OH and $-$O$-$ groups. We build 2D supercells with $n_S = 8$ carbon sites: as illustrated in Fig. 1 hydroxyls can be adsorbed at each carbon site, while an epoxy groups can bridge each of the $n_B = 12$ carbon-carbon bonds. We restrict the possible arrangements of oxygen-containing groups to those that fulfill the following conditions: (i) carbon atoms should be three- or fourfold-coordinated after adsorption, and (ii) hydroxyl groups cannot be adsorbed on first-nearest-neighbor atomic sites on the same side of the graphene basal plane. These conditions allow to exclude irrelevant atomic arrangements with extremely high formation energies, as previously demonstrated in Ref.[39] The described constraints lead to a final set of 16343 possible supercells, including 8 carbon atoms, $n_{\mathrm{OH},j}$ $-$OH groups and $n_{\mathrm{O},j}$ $-$O$-$ groups. These configurations can be reorganized in J =308 symmetry equivalent classes with degeneracies g_j, accounting for all possible symmetry operations. For further discussion of specific atomic arrangements, an example of the configuration labeling procedure is give in the captions of Fig. 1.

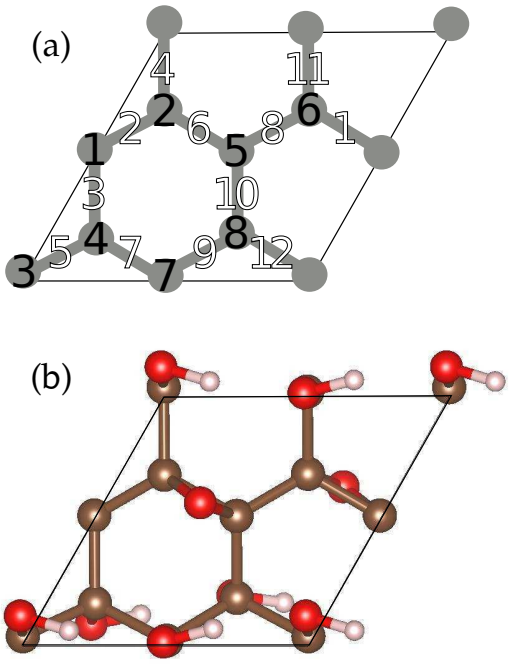

Figure 1: (Color online) (a) The atomic sites and the carbon-carbon bonds are labeled with integer numbers from 1 to 8 (in black) and 1 to 12 (in white), respectively. The configuration label is obtained by combining the 8 atomic site labels and the 12 carbon-carbon bond labels. Sites without oxygen groups are represented as 0, oxygen groups above the graphene layer as "u" and oxygen groups below the graphene layer as "d". (b) An example of a cluster configuration. Carbon, oxygen and hydrogen are respectively illustrated by brown, red and white spheres. According to the labeling system described in (a), the configuration of the represented atomic arrangement is 00ud00ud-d0000u000000.

Each cluster arrangement is then treated as a unit cell of an artificial 2D crystal obtained from a repetition of the considered cluster over the whole graphene basal plane. Then, a set of physical properties P_j is calculated for each cluster system j. The chemical composition of the graphene oxide samples is described by the fractions x, y, and z (with $x+y+z=1$), which are defined as the fractions of carbon atoms that are bonded only to carbon atoms, to hydroxyl groups, and to epoxy groups, respectively. The average stoichiometry of the compound be expressed as $\mathrm{CO}_{y+z/2}\mathrm{H}_y$.

Let $x_j(x,y,T)$, where $j=1,2,\ldots,J$, be the distribution of occurrence probability of the cluster class j in a realized GO sample with average chemical composition x, y, and at the growth temperature T. If the total number of clusters is M, and the cluster class j contains M_j equivalent clusters, the probability of occurrence x_j is equal to $x_j = M_j/M$. In a solid

under normal pressure (1 atm) the Gibbs free energy of mixing can be approximated by the mixing Helmholtz free energy $\Delta F = \Delta U - T\Delta S$.[40] ΔU is the internal energy and it can be written as

$$\Delta U = \sum_{i=1}^{J} M_j E_j - M(xE_{\mathrm{C}} + yE_{\mathrm{COH}} + zE_{\mathrm{CO}_{1/2}}), \tag{1}$$

where E_j, E_{C}, E_{COH}, and $E_{\mathrm{CO}_{1/2}}$ are the total energies of the cluster configuration j, the cluster of pristine graphene (C), the cluster of graphene with complete hydroxyl coverage (COH), and the cluster of graphene fully decorated with epoxy groups ($\mathrm{CO}_{1/2}$). The configurational entropy ΔS is calculated from the expression of the Shannon entropy as a function of the probability distribution x_j and degeneracies g_j as[39]

$$\Delta S = k_b M \sum_{j=1}^{J} x_j(\ln g_j - \ln x_j), \tag{2}$$

where k_b is the Boltzmann constant.

Finally, the distribution of occurrence probability x_j for the different cluster classes is determined by minimization of the Helmholtz free energy. The probability distribution x_j must fulfill some constraints: (i) the normalization of the total probability, $\sum_{j=1}^{J} x_j = 1$, and (ii) the definition of average chemical composition, $\sum_{j=1}^{J} x_j n_{\mathrm{OH},j} = \overline{n_{\mathrm{OH}}}$ and $\sum_{j=1}^{J} x_j n_{\mathrm{O},j} = \overline{n_{\mathrm{O}}}$, where $\overline{n_{\mathrm{OH}}} = 8y$ and $\overline{n_{\mathrm{O}}} = 4z$ are the average number of hydroxyl and epoxy groups per cluster in a $\mathrm{CO}_{y+z/2}\mathrm{H}_y$ system. This constrained minimization is equivalent to that of a ternary alloy obtained by mixing C, COH, and $\mathrm{CO}_{1/2}$, as described in Ref.[43] The constrained minimization leads to the distribution of occurrence probability

$$x_j = \frac{g_j \lambda_1^{n_{\mathrm{OH},j}} \lambda_2^{n_{\mathrm{O},j}} \exp\left(-\frac{E_j}{k_B T}\right)}{\sum_{j=1}^{J} g_j \lambda_1^{n_{\mathrm{OH},j}} \lambda_2^{n_{\mathrm{O},j}} \exp\left(-\frac{E_j}{k_B T}\right)}, \tag{3}$$

where λ_1 and λ_2 are two numerical constants obtained as Lagrange multipliers in the constrained minimization problem. They can be calculated by solving the pair of polynomial

equations

$$\sum_{j=1}^{J} g_j(n_{\mathrm{OH},j} - \overline{n_{\mathrm{OH}}})\lambda_1^{n_{\mathrm{OH},j}}\lambda_2^{n_{\mathrm{O},j}}\exp\left(-\frac{E_j}{k_B T}\right) = 0, \tag{4}$$

$$\sum_{j=1}^{J} g_j(n_{\mathrm{O},j} - \overline{n_{\mathrm{O}}})\lambda_1^{n_{\mathrm{OH},j}}\lambda_2^{n_{\mathrm{O},j}}\exp\left(-\frac{E_j}{k_B T}\right) = 0. \tag{5}$$

After that the occurrence probabilities are calculated with Eq. (3), any average physical or chemical property $\overline{P}$ of the disordered system can be estimated as an average of the properties of the individual clusters P_j, weighted by the corresponding occurrence probabilities x_j:[40]

$$\overline{P} = \sum_{j=1}^{J} x_j P_j. \tag{6}$$

Ab initio calculations

The input data for our statistical model are obtained from *ab initio* calculations based on density functional theory (DFT), as implemented in the VASP.[44,45] We use the generalized gradient approximation (GGA), as proposed by Perdew-Burke-Ernzerhof (GGA-PBE),[46,47] to calculate the exchange and correlation (XC) functional. The pseudopotentials of C, O and H atoms are generated within the Projector-Augmented Wave (PAW) method.[48,49] The kinetic-energy cutoff of the plane-wave basis is set as 450 eV.

The total energy calculations are performed using a 9x9x1 Γ-centered Monkhorst-Pack k-point grid to compute the integrals over the Brillouin zone (BZ).[50] In order to find the equilibrium configuration, all atomic coordinates are relaxed until the Hellmann-Feynman forces are smaller than 0.01 eV Å^{-1} within a spin-unpolarized formalism. The 2D systems are simulated by the repetition of the considered cluster in the three dimensions, with a spacing of $L = 20$ Å between two neighboring graphene planes to avoid spurious interactions.

The Kohn-Sham band gap calculated from DFT using standard exchange-correlation functionals is strongly underestimated.[51] However, one can extract a a qualitatively correct

dependence of the energy gap and bowing parameters on the chemical composition.[28,29,52] This fact has also been confirmed in our recent study of adsorption of different oxygen-containing groups on graphene.[39] Due to the large number of configurations considered and the significant enhancement of computer cost required by more sophisticated methods for accurate quasiparticle states, we focus on the qualitative behavior of the average energy gap to analyze the dependence of electronic properties on the chemical composition of GO. The atomic arrangements that give rise to metallic properties are attributed a zero band gap value in the calculation of statistical averages.

Optical properties are described by the frequency-dependent dielectric matrix, which is calculated within the independent-quasiparticle approximation.[53] The optical transition matrix elements $M_{cv}(\vec{k}, \hat{q})$ are described adopting the longitudinal gauge.[54] The in-plane dielectric function allows the computation of the 2D optical absorbance $A_j(\omega)$ for normal incidence as defined in Ref.:[55]

$$A_j(\omega) = \frac{\omega}{c} L \, Im[\epsilon_{kk}(\omega)] \; (k = x, y), \tag{7}$$

where c is the speed of light in vacuum. An accurate calculation of absorption spectra would require the inclusion of quasiparticle corrections and excitonic effects.[56] However, a tendency for compensation of these two effects has been demonstrated for graphene,[57] and insulating 2D systems such as hBN.[58] Therefore, a good qualitative picture of the dependence of the optical properties on the chemical composition can be obtained within the independent quasiparticle approximation for our disordered 2D system.[29]

Results and discussion

Thermodynamic stability

The energetics of the clusters classes is investigated by defining the excess total energy of each atomic arrangement as

$$\Delta E_j = E_j - \frac{n_{\mathrm{C},j}}{8} E_{\mathrm{C}} - \frac{n_{\mathrm{OH},j}}{8} E_{\mathrm{COH}} - \frac{n_{\mathrm{O},j}}{4} E_{\mathrm{CO}_{1/2}}, \tag{8}$$

where $n_{\mathrm{C},j}$ represents the number of three-fold coordinated carbons in the cluster class j. The expression (8) represents the formation energy of a cluster class j, with respect to the three end components: pure graphene with total energy E_{C}, fully oxidized GO with only $-$OH groups and energy E_{OH}, and fully oxidized GO with only $-$O$-$ groups and energy $E_{\mathrm{CO}_{1/2}}$. The atomic geometry of the end components are displayed in Figs. 2 a, b, and c, for graphene (x=1), a cluster fully decorated with hydroxyl (y=1), and 00000000-00ud00000ud0, the cluster class with four epoxy groups per cluster (z=1) and the lowest internal energy, respectively. Configurations with large excess total energies ΔE_j are inhibited by the minimization of the Helmholtz free energy of mixing. They are realized only at high growth temperatures, while configurations with negative formation energy indicate that such atomic arrangements are thermodynamically favored and realized even at low temperatures.

In our previous work,[39] we reported only positive excess energies for oxidation of graphene sheets with only hydroxyl or epoxy groups, which respectively correspond to $z = 0$ and $y = 0$. In these two limit cases, the GO system tends to decompose into oxygen-poor and -rich domains. Here, we investigate the simultaneous oxidation with $-$OH and $-$O$-$ groups and explore new features that emerge from the interaction between both oxygen-containing groups.

The vast majority of cluster configurations still exhibits positive excesses energies, especially for understoichiometric configurations. However, eight different classes of fully oxidized configurations with hydroxyl and epoxy groups exhibit negative excess energies, indicating

great energetic stability even at low temperatures. These configurations are tabeled in Table 1. Four configurations with negative excess energies occur at $(n_{C,j}/8, n_{OH,j}/8, n_{O,j}/4) = (0, 0.5, 0.5)$, corresponding to four $-$OH and two $-$O$-$ groups per 8-carbon cluster. The other four energetically favorable arrangements occur at $(n_{C,j}/8, n_{OH,j}/8, n_{O,j}/4) = (0, 0.25, 0.75)$, corresponding to two $-$OH and three $-$O$-$ per cluster. These findings agree with the indication of highly oxidized domains with simultaneous adsorption of hydroxyl and epoxy groups by nuclear magnetic resonance measurements,[19] and also with other theoretical works that indicate the total energies are considerably lowered when epoxy and hydroxyl groups are adsorbed together.[37,38] Oxidized domains with both hydroxyl and epoxy groups are, therefore, thermodynamically favored over a spatial segregation of the oxygen-containing groups. The lowest energy configurations at $(n_{C,j}/8, n_{OH,j}/8, n_{O,j}/4) = (0, 0.5, 0.5)$ and $(0, 0.25, 0.75)$ are u0d00d0u-00000ud00000 and d000000d-0000uu0000u0, respectively, which are illustrated in Figs. 2 d and e.

Table 1: Cluster labels, their numbers of hydroxyl (epoxy) groups per cluster $n_{OH,j}$ ($n_{epo,j}$), degeneracies g_j, and excess energies ΔE_j. All the configurations with negative excess energy are listed.

Label	$n_{OH,j}$	$n_{epo,j}$	g_j	ΔE_j (eV/cluster)
du000000-000000uu000d	2	3	96	-0.40
u0000d00-00000uu0000d	2	3	48	-0.03
d000000d-0000uu0000u0	2	3	16	-0.67
d000000d-0000uu0000d0	2	3	48	-0.12
du0ud000-0000000000ud	4	2	48	-0.47
udud0000-000000000ud0	4	2	48	-0.58
u0u00d0d-00000ud00000	4	2	24	-0.29
u0d00d0u-00000ud00000	4	2	24	-0.72

The thermodynamic stability of the ternary system with respect to its chemical composition is investigated by calculating the mixing free energy $\Delta F(x, y, T)$ at typical growth temperatures of 200^oC and 1100^oC,[6,59–61] considering the whole composition range $x = 1-y-z$, y, and z. The results are represented by the two color maps depicted in Fig. 3. The most favorable configurations of the end components C (graphene), COH (GO with hydroxyl),

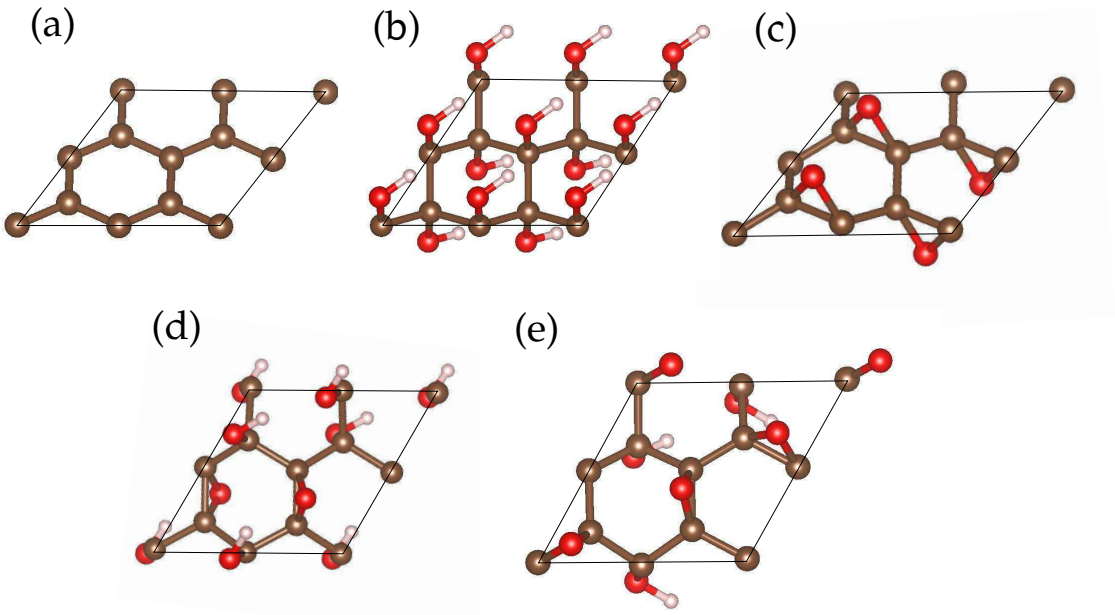

Figure 2: (Color online) Important cluster configurations representing (a) pristine graphene, (b) COH, (c) 00000000-00ud00000ud0, the lowest-energy cluster fully oxidized by epoxy groups, (d) u0d00d0u-00000ud00000, with ΔE_j =-0.72 eV/cluster, and (e) d000000d-0000uu0000u0, with ΔE_j =-0.67 eV/cluster.

and $CO_{1/2}$ (GO with epoxy) are chosen as the corner points of the displayed triangles. Their edges of the triangle correspond to the variation of one single parameter (x, y, or z), while the other two are set to zero. The adsorption processes with single oxygen-containing group species, which correspond to the C−COH and C−$CO_{1/2}$ edges of the color maps, exhibit positive mixing energies for the considered growth temperatures, indicating a strong tendency to phase decomposition, understood here as the agglomeration of the functionalizing groups (see our previous results reported in Ref.[39]). The red and orange areas indicate an enhancement of the mixing free energy, and, therefore, a strong tendency to phase decomposition into pristine graphene (C vertex) and fully oxidized domains with both oxygen-containing groups ($CO_{1/2}$-COH edge) is indicated. When higher temperatures are considered, the entropy term becomes more important and contributes to the system stability at intermediate oxidation level. These results are in agreement with other theoretical investigations[37,38,62] and experimental findings, that point to the presence of non-oxidized domains in GO samples.[16,63]

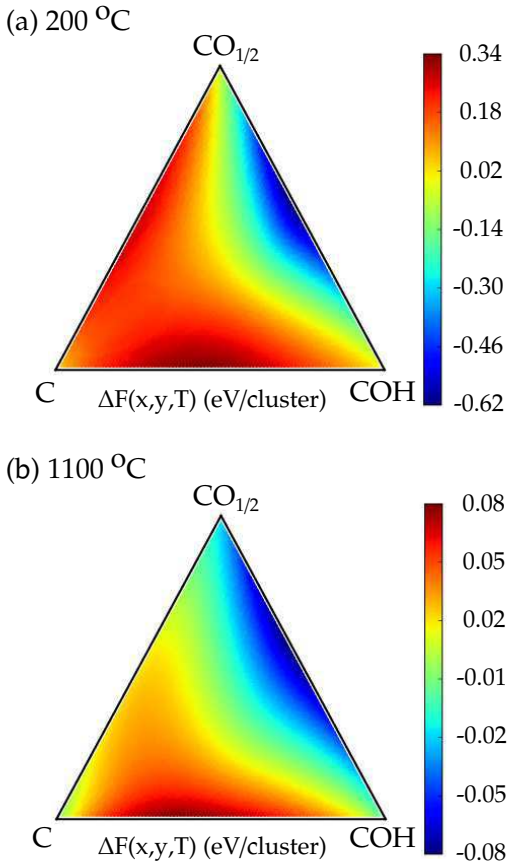

Figure 3: (Color online) The mixing free energy of the understoichiometric GO systems as a function of the average compositions at a synthesis temperature of (a) 200^oC and (b) 1100^oC.

The reasons for the increase of the mixing free energy along the COH$-$CO$_{1/2}$ edges of the color maps of Fig. 3 are illustrated in Fig. 4. The mixing free energy ΔF is decomposed into the internal energy contribution ΔU and the configurational entropy term $-T\Delta S$. The mixing free energy ΔF is dominated by the entropy contribution $-T\Delta S$ at high temperatures. However, at low temperatures, the occurrence of atomic arrangements with negative excess energies strongly affects ΔU. Accounting for the cluster statistics, fully oxidized domains decorated with hydroxyl and epoxy groups turn out to be stable at the considered growth temperatures.

In the hydroxyl-rich limit ($y \rightarrow 1$), nearly all clusters correspond to the COH end component. This situation leads to $\Delta U = 0$, while an entropy per cluster of $\Delta S = k_b \ln(2)$ is calculated by the cluster expansion, since $g_{COH} = 2$. In the GQCA picture, the COH clusters

are free to 'flip' independently from the oxygen-containing groups in the neighborhood, due to the assumed energetic and statistical independence between the clusters. In the epoxy-rich limit ($z \to 1$) there is a competition between different possible epoxy arrangements in the sheets. At low temperature (see the solid lines in Fig. 4), the configurations with lower internal energy of mixing are strongly favored, yielding low ΔU and ΔS. As the temperature increases, the occurrence probability of cluster classes corresponding to more energetic configurations is enhanced, leading to larger ΔU and $T\Delta S$ contributions to the total excess free energy.

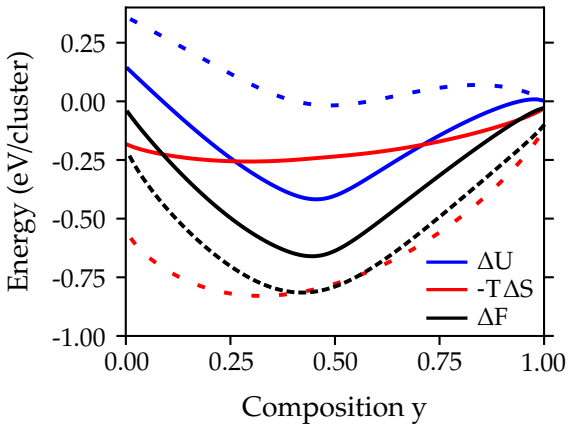

Figure 4: (Color online) The internal energy ΔU, the entropic contribution to the free energy $-T\Delta S$, and the Helmholtz free energy of mixing ΔF for a fully oxidized system $(\mathrm{COH})_y(\mathrm{CO}_{1/2})_{1-y}$. Solid lines are obtained at a growth temperature of 200^oC, while dashed lines indicate a growth temperature of 1100^oC.

Structural properties

We obtained the lattice constants of $a_{\mathrm{C}} = 2.47$ Å, $a_{\mathrm{COH}} = 2.63$ Å and $a_{\mathrm{CO}_{1/2}} = 2.57$ Å for the pure end compounds. A maximum lattice mismatch of 7% is calculated between graphene, and GO with only $-$OH groups. The average lattice constants $a(y, z, T)$ of the GO systems as a function of the chemical parameters are calculated within the GQCA statistics and depicted in Fig. 5. A gradual change between the end component lattice constant is observed and the linear fit $a = xa_{\mathrm{C}} + ya_{\mathrm{COH}} + za_{\mathrm{CO}_{1/2}}$ gives the calculated lattice constant

with a maximal error below 1.5% at both considered temperatures. That means that the Vegard's law is widely fulfilled.

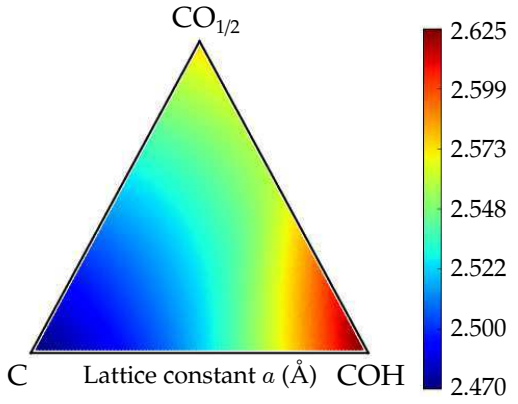

Figure 5: (Color online) The average lattice constant a of the GO systems calculated within the GQCA approach as the second-nearest neighbor C distance. A synthesis temperature of 200^oC is considered.

The buckling amplitude $\Delta(y, z, T)$ of the carbon sheet is also investigated. The graphene layer exhibits a honeycomb planar structure with $\Delta_j = 0.00$ Å , while the COH system shows a buckling amplitude of $\Delta_j = 0.51$ Å , which is associated with a pure sp^3 hybridization of the carbon atomic orbitals. The $CO_{1/2}$ end component fully decorated by epoxy groups undergoes a different distortion of the planar honeycomb structure, depending on how the epoxy groups are distributed. Buckling amplitudes between $\Delta_j = 0.00$ Å and 0.50 Å are observed, that results in an average buckling amplitude of 0.36 Å for the considered range of temperatures. The dependence of the average buckling amplitude $\Delta(y, z, T)$ on the chemical compositions at 200°C is displayed in Fig. 6. A slight dependence of the temperature is observed, however the qualitative behavior of the amplitude with the GO chemical content remains the same at 1100 °C.

One observes a pronounced maximum buckling amplitude of 0.71 Å for graphene oxide fully oxidized with both oxygen-containing groups in proportions near $n_{\mathrm{OH}}/n_{\mathrm{O}} = 1$. This value of the buckling is is larger than any buckling amplitude observed for the end components. This is the result of large statistical contributions of the configurations u0d00d0u-00000ud00000 and udud0000-000000ud0, which are thermodynamically favored due to their

negative excess energies ($\Delta E_j = -0.72$ and -0.58 ev/cluster, respectively). They exhibit buckling amplitudes significantly larger than the pure sp^3 buckling ($\Delta_j = 0.75$Å and 0.62, respectively), as some $-$OH/$-$O$-$ distributions induce low energy long-range distortions of the planar honeycomb structure.

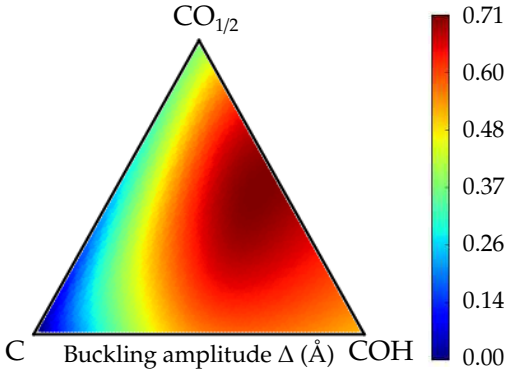

Figure 6: (Color online) The average buckling amplitude Δ of the GO systems calculated within the GQCA approach at a synthesis temperature of 200^oC.

The most stable configuration at $(x, y, z) = (0, 0.5, 0.5)$ reveals alternated stripes of carbon atoms bound to hydroxyl and epoxy groups, as illustrated in Fig. 2(d). The most stable configuration at $(x, y, z) = (0, 0.25, 0.75)$ is a newly discovered favorable structure, made of hexagons of carbon atoms attached to epoxy groups, surrounded by carbon atoms attached to $-$OH groups. This pattern can be verified by building a 2D-periodic repetition of the cluster of Fig. 2(e).

Electronic and optical properties

We calculated the electronic and optical properties of the 308 cluster configurations using the GGA-PBE exchange and correlation functional. The DFT Kohn-Sham fundamental band gaps have values of $E_{g,\mathrm{C}} = 0$ eV, $E_{g,\mathrm{COH}} = 2.25$ eV, and $E_{g,\mathrm{CO_{1/2}}} = 4.00$ eV at 200 ^{o}C for the considered end components. We demonstrated that in case of adsorption of only one oxygen-containing group on graphene the Kohn-Sham energy gaps obtained from GGA-PBE calculations show the same trends as those computed with more accurate screened hybrid functionals.[39]

The fundamental energy gap depends on the stoichiometry, i.e., the general oxidation state of GO. We can therefore consider the average gap $E_g(y, z, T)$ as a function of the parameters y and z, related to oxidation by hydroxyl and epoxy groups, respectively and on the growth temperature T. The average gap is not a simple weighted average of the band gaps of the end materials, and the deviation from this simple linear behavior gives the so-called gap bowing $\Delta E_g(y, z, T)$, defined as

$$E_g(y, z, T) = xE_{g,\mathrm{C}} + yE_{g,\mathrm{COH}} + zE_{g,\mathrm{CO_{1/2}}} + \Delta E_g(y, z, T). \quad (9)$$

An estimate of the absolute values of the energy gap can be made by applying a scissor operator approximation, considering quasiparticle corrections to the fundamental energy gaps of the COH and $CO_{1/2}$, and the gap bowing estimated from the GGA-PBE calculations. The average gaps are calculated within GQCA at 200^oC and 1100^oC. The energy gap bowings $\Delta E_g(y, z, T)$ obtained using the gaps $E_{g,j}$ for each configuration class j and the formula (6), inserting the statistical weighs x_j at the considered growth temperatures are depicted using color maps in Fig. 7.

In agreement with previous results for graphene oxide systems decorated with single oxygen-containing groups,[39] the band gap bowing for $-$O$-$ rich oxidation does not significantly change when the temperature increases, while the band gap bowing for $-$OH rich oxidation changes from regular bowing ($\Delta E_g < 0$) at 200^oC to a profile that may exhibit regular bowing or anti-bowing ($\Delta E_g > 0$) at 1100^oC, depending on the oxidation level of the system. The gap bowings along the C$-$$CO_{1/2}$ edge can be written as $\Delta E_g(x, T) = -b(T)x(1 - x)$, while along the C$-$COH edge the gap may exhibit positive and negative bowing depending on the chemical composition at large growth temperatures (see[39]).

The energy gap bowing along the $CO_{1/2}-$COH edge ($y = 1 - z$), i.e., for the simultaneous deposition of $-$OH and $-$O$-$ groups in the limit of complete oxidation, is larger for fully oxidized systems with $-$O$-$/$-$OH ratios between 1 and 3, at both growth temperatures. This enhancement of the energy gaps is explained by the significant contributions of

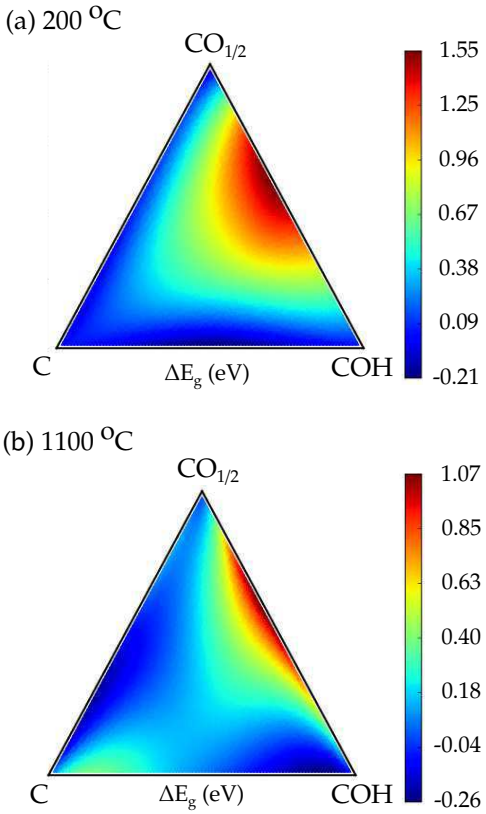

Figure 7: (Color online) The average energy gap bowing of the GO systems as a function of the average compositions at a growth temperature of (a) 200^oC and (b) 1100^oC.

favorable configurations with negative excess energies and large energy gap values, e.g., 4.40 eV (u0d00d0u−00000ud00000) and 4.68 eV (d000000d−0000uu0000u0). Significant changes can be observed at different temperatures. The application of the statistical approach on a larger set of configurations results hence into an even larger energy gap range for band gap engineering than the one obtained by Yan *et al.*[37,38] These authors had in fact reported an energy gap bowing between 0.8-1.1 eV for fully oxidized configurations, when the system is prepared at low growth temperature.

The increase of the growth temperature induces more configurational disorder in the GO system and the contributions of the configurations with lower energies decrease with the rising temperature. A signature of this effect is the shrinkage of the red area in Fig. 7(b), compared with Fig. 7(a). This result shows the big potential of graphene oxide to provide a 2D platform for novel 2D electronics, whose electronic properties can be tuned controlling

both the chemical composition and growth conditions. Thereby, the coadsorption of hydroxyl and epoxy groups paves the way for improved tuning strategies, not only in the limit of full oxidation but also in the intermediate regime, with structures similar to those in Figs. 2 d and e.

The gap bowing $\Delta E_g(y,z,T)$ illustrated in Fig. 7 can be fitted with the following expression

$$\Delta E_g(y,z,T) = c_0 + c_1(1-x)yz + c_2(1-y)zx + (1-z)xy(c_3x + c_4y) + c_5xyz, \quad (10)$$

where c_0, c_1, c_2, c_3, c_4, and c_5 are parameters calculated by minimizing the total squared error. We calculated these fitting parameters for T =300 K, 473 K, 1000 K, and 1473 K using Nelder-Mead algorithm.[64] The obtained coefficients and the fitting average error at each temperature are listed in Table 2. The maximal error for all considered chemical compositions and temperatures was 0.27 eV.

Table 2: Fitting parameters for gap bowing $\Delta E_g(y,z,T)$ as defined in Eq.10 for different growth temperatures. The average fitting error $\bar{e}$ is given for each temperature. Parameters for intermediate temperatures can be estimated by interpolation.

Temperature (K)	c_0	c_1	c_2	c_3	c_4	c_5	$\bar{e}$ (eV)
300	0.01	5.87	0.32	0.03	-4.52	16.60	0.09
473	0.04	5.76	0.18	-0.04	-2.31	9.44	0.04
1000	0.08	4.78	0.07	2.30	-2.36	0.11	0.07
1373	0.08	4.28	0.11	3.22	-3.54	-2.39	0.07

The dependence of the optical absorbance on the $-$O$-$/$-$OH ratio of a fully oxidized system is represented in Fig. 8. The spectra $A_j(\omega)$ for all cluster classes have been computed in the independent-quasiparticle approximation and averaged using the probabilities $x_j(y,z,T)$ in (6). One observes that the temperature increase does not strongly affect the optical absorption of GO in the fully oxidized limit with co-adsorption of $-$OH and $-$O$-$ groups. This insensitivity suggests that the statistics is dominated by the low energy con-

figurations in a wide temperature range. One also observes that the first pronounced peak in the optical absorbance for intermediate compositions $y \approx z \approx 0.5$ is blue shifted for very large photon energies (above 7 eV). This observation is consistent with the large anti-bowing coefficients observed in Fig. 7 for such compositions. The strength of light absorption decreases, however, monotonically moving from the case of full decoration by epoxy groups to the case of hydroxyl covered graphene.

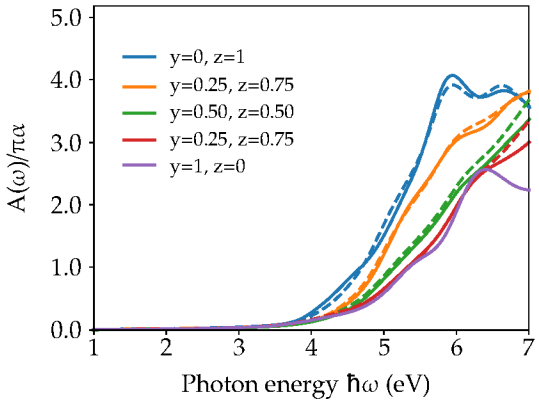

Figure 8: (Color online) The average optical absorbance of fully oxidized GO systems for different $-$O$-$/$-$OH ratio measured in units of $\pi\alpha$ (α - fine structure constant). The full lines represent the averages obtained within the GQCA statistical approach considering a growth temperature of 200^oC, while the dashed lines have been computed at a growth temperature of 1100^oC. The corresponding O/C ratio of each curve is given by $(y + z/2)$.

Summary

We studied graphene oxide obtained by simultaneous adsorption of hydroxyl and epoxy groups on graphene and focused attention on effects that emerge from the coexistence of both oxygen-containing groups on the graphene sheet. To this end, we extended the generalized quasichemical approximation to the case of co-adsorption of two different functionalizing groups on a 2D sheet. Within this statistical approach we performed *ab initio* calculations of structural, electronic and optical properties based on density functional theory.

We showed that the phase separation of the system into carbon- and oxygen-rich phases is thermodynamically favored when hydroxyl and epoxy groups are adsorbed at the same

time on graphene. This is similar to what happens when only one oxygen-containing group is considered. The investigation of the system energetics proved that a random distribution of functionalizing groups in the oxygen-rich domains is observed at typical growth temperatures. We could identify favored fully oxidized ordered arrangements of hydroxyl and epoxy groups with negative excess energy. Moreover, we revealed how the density and the arrangement of the oxygen-containing groups control buckling amplitude of the carbon basal sheet. The chemical composition and atomic arrangements also significantly influence the average fundamental energy gap and the band gap bowing. In case of a full oxidation with equal concentration of $-$OH and $-$O$-$ groups a strong antibowing is found, and it is explained as a consequence of the large band gaps calculated for the favored atomic geometries identified in this work. Finally, we discussed the dependence of the optical absorbance on composition and temperature of a fully oxidized GO phase and demonstrated a strong influence of the relative amount of $-$OH and $-$O$-$ groups on the calculated properties.

These results offer valuable insight into the structure of disordered graphene oxide samples, and support the experimental attempts to obtain samples with defined chemical composition, a sufficient phase stability and the average properties of the disordered system.

Acknowledgement

We thank the Brazilian funding agencies FAPESP (Grant n. 2012/50738-3), CAPES (PVE - Grants n. 88881.068355/2014-1, and 88887.116535/2016-00), and CNPQ (Grants n. 305405/2014-4, and 308742/2016-8) for the financial support. The authors acknowledge the National Laboratory for Scientific Computing (LNCC/MCTI, Brazil) for providing HPC resources of the SDumont supercomputer. Computational resources were also provided by the Leibniz Supercomputing Centre through the projects pr62ja. I. Guilhon is grateful to the hospitality of the Friedrich-Schiller University.

References

(1) Geim, A. K.; Novoselov, K. S. The Rise of Graphene. *Nature Mat.* **2007**, *6*, 183.

(2) Park, S.; Ruoff, R. S. Chemical Methods for the Production of Graphenes. *Nature Nano* **2009**, *4*, 217.

(3) Eigler, S.; Hirsch, A. Chemistry with Graphene and Graphene Oxide-Challenges for Synthetic Chemists. *Angewandte Chemie International Edition* **2014**, *53*, 7720–7738.

(4) Loh, K. P.; Bao, Q.; Eda, G.; Chhowalla, M. Graphene Oxide as a Chemically Tunable Platform for Optical Applications. *Nature Chemistry* **2010**, *2*, 1015–1024.

(5) Mao, S.; Pu, H.; Chen, J. Graphene Oxide and its Reduction: Modeling and Experimental Progress. *RSC Adv.* **2012**, *2*, 2643–2662.

(6) Dreyer, D. R.; Park, S.; Bielawski, C. W.; Ruoff, R. S. The Chemistry of Graphene Oxide. *Chem. Soc. Rev.* **2010**, *39*, 228–240.

(7) Pulci, O.; Gori, P.; Marsili, M.; Garbuio, V.; Del Sole, R.; Bechstedt, F. Strong Excitons in Novel Two-dimensional Crystals: Silicane and Germanane. *EPL (Europhysics Letters)* **2012**, *98*, 37004.

(8) Robinson, J. T.; Perkins, F. K.; Snow, E. S.; Wei, Z.; Sheehan, P. E. Reduced Graphene Oxide Molecular Sensors. *Nano Letters* **2008**, *8*, 3137–3140.

(9) Dua, V.; Surwade, S.; Ammu, S.; Agnihotra, S.; Jain, S.; Roberts, K.; Park, S.; Ruoff, R.; Manohar, S. All-Organic Vapor Sensor Using Inkjet-Printed Reduced Graphene Oxide. *Angewandte Chemie* **2010**, *122*, 2200–2203.

(10) Gómez-Navarro, C.; Weitz, R. T.; Bittner, A. M.; Scolari, M.; Mews, A.; Burghard, M.; Kern, K. Electronic Transport Properties of Individual Chemically Reduced Graphene Oxide Sheets. *Nano Letters* **2007**, *7*, 3499–3503.

(11) Wei, Z.; Wang, D.; Kim, S.; Kim, S.-Y.; Hu, Y.; Yakes, M. K.; Laracuente, A. R.; Dai, Z.; Marder, S. R.; Berger, C. et al. Nanoscale Tunable Reduction of Graphene Oxide for Graphene Electronics. *Science* **2010**, *328*, 1373–1376.

(12) Wu, X.; Sprinkle, M.; Li, X.; Ming, F.; Berger, C.; de Heer, W. A. Epitaxial-Graphene/Graphene-Oxide Junction: An Essential Step Towards Epitaxial Graphene Electronics. *Phys. Rev. Lett.* **2008**, *101*, 026801.

(13) Zhang, J.; Zhao, X. S. Conducting Polymers Directly Coated on Reduced Graphene Oxide Sheets as High-Performance Supercapacitor Electrodes. *The Journal of Physical Chemistry C* **2012**, *116*, 5420–5426.

(14) Brodie, B. C. On the Atomic Weight of Graphite. *Philosophical Transactions of the Royal Society of London* **1859**, *149*, 249–259.

(15) He, H.; Riedl, T.; Lerf, A.; Klinowski, J. Solid-State NMR Studies of the Structure of Graphite Oxide. *The Journal of Physical Chemistry* **1996**, *100*, 19954–19958.

(16) He, H.; Klinowski, J.; Forster, M.; Lerf, A. A New Structural Model for Graphite Oxide. *Chemical Physics Letters* **1998**, *287*, 53 – 56.

(17) Hofmann, U.; Holst, R. Über die Saeurenatur und die Methylierung von Graphitoxyd. *Berichte der deutschen chemischen Gesellschaft (A and B Series)* **1939**, *72*, 754–771.

(18) Ruess, G. Über das Graphitoxyhydroxyd (Graphitoxyd). *Monatshefte für Chemie und Verwandte Teile Anderer Wissenschaften* **1947**, *76*, 381–417.

(19) Cai, W.; Piner, R. D.; Stadermann, F. J.; Park, S.; Shaibat, M. A.; Ishii, Y.; Yang, D.; Velamakanni, A.; An, S. J.; Stoller, M. et al. Synthesis and Solid-State NMR Structural Characterization of 13C-Labeled Graphite Oxide. *Science* **2008**, *321*, 1815–1817.

(20) Nourbakhsh, A.; Cantoro, M.; Vosch, T.; Pourtois, G.; Clemente, F.; van der

Veen, M. H.; Hofkens, J.; Heyns, M. M.; Gendt, S. D.; Sels, B. F. BandGap Opening in Oxygen Plasma-treated Graphene. *Nanotechnology* **2010**, *21*, 435203.

(21) Kim, M. C.; Hwang, G. S.; Ruoff, R. S. Epoxide Reduction with Hydrazine on Graphene: A First Principles Study. *The Journal of Chemical Physics* **2009**, *131*, 064704.

(22) Ci, L. Atomic Layers of Hybridized Boron Nitride and Graphene Domains. *Nature Material* **2010**, *9*, 430–435.

(23) Uddin, M. R.; Majety, S.; Li, J.; Lin, J. Y.; Jiang, H. X. Layer-Structured Hexagonal (BN)C Semiconductor Alloys with Tunable Optical and Electrical Properties. *Journal of Applied Physics* **2014**, *115*, 093509.

(24) Uddin, M. R.; Li, J.; Lin, J. Y.; Jiang, H. X. Carbon-rich Hexagonal (BN)C Alloys. *Journal of Applied Physics* **2015**, *117*, 215703.

(25) Li, H.; Duan, X.; Wu, X.; Zhuang, X.; Zhou, H.; Zhang, Q.; Zhu, X.; Hu, W.; Ren, P.; Guo, P. et al. Growth of Alloy MoS2xSe2(1-x) Nanosheets with Fully Tunable Chemical Compositions and Optical Properties. *Journal of the American Chemical Society* **2014**, *136*, 3756–3759.

(26) Chen, Y.; Xi, J.; Dumcenco, D. O.; Liu, Z.; Suenaga, K.; Wang, D.; Shuai, Z.; Huang, Y.-S.; Xie, L. Tunable Band Gap Photoluminescence from Atomically Thin Transition-Metal Dichalcogenide Alloys. *ACS Nano* **2013**, *7*, 4610–4616.

(27) Zheng, Z.; Yao, J.; Yang, G. Centimeter-Scale Deposition of Mo0.5W0.5Se2 Alloy Film for High-Performance Photodetectors on Versatile Substrates. *ACS Applied Materials & Interfaces* **2017**, *9*, 14920–14928.

(28) Guilhon, I.; Teles, L. K.; Marques, M.; Pela, R. R.; Bechstedt, F. Influence of Structure

and Thermodynamic Stability on Electronic Properties of Two-dimensional SiC, SiGe, and GeC Alloys. *Phys. Rev. B* **2015**, *92*, 075435.

(29) Guilhon, I.; Marques, M.; Teles, L. K.; Bechstedt, F. Optical Absorbance and Band-Gap Engineering of $(BN)_{1-x}(C_2)_x$ Two-dimensional Alloys: Phase Separation and Composition Fluctuation Effects. *Phys. Rev. B* **2017**, *95*, 035407.

(30) Padilha, J. E.; Seixas, L.; Pontes, R. B.; da Silva, A. J. R.; Fazzio, A. Quantum Spin Hall Effect in a Disordered Hexagonal SixGe1-x Alloy. *Phys. Rev. B* **2013**, *88*, 201106.

(31) Akiyama, T.; Yoshimura, G.; Nakamura, K.; Ito, T. Theoretical Investigations on the Stability and Electronic Structures of Two-dimensional Group-IV Ternary Alloy Monolayers. *Journal of Vacuum Science & Technology B, Nanotechnology and Microelectronics: Materials, Processing, Measurement, and Phenomena* **2017**, *35*, 04F103.

(32) Gao, H.; Wang, L.; Zhao, J.; Ding, F.; Lu, J. Band Gap Tuning of Hydrogenated Graphene: H Coverage and Configuration Dependence. *The Journal of Physical Chemistry C* **2011**, *115*, 3236–3242.

(33) Haberer, D.; Vyalikh, D. V.; Taioli, S.; Dora, B.; Farjam, M.; Fink, J.; Marchenko, D.; Pichler, T.; Ziegler, K.; Simonucci, S. et al. Tunable Band Gap in Hydrogenated Quasi-Free-Standing Graphene. *Nano Letters* **2010**, *10*, 3360–3366.

(34) Meduri, P.; Chen, H.; Xiao, J.; Martinez, J. J.; Carlson, T.; Zhang, J.-G.; Deng, Z. D. Tunable Electrochemical Properties of Fluorinated Graphene. *J. Mater. Chem. A* **2013**, *1*, 7866–7869.

(35) Karlicky, F.; Kumara Ramanatha Datta, K.; Otyepka, M.; Zboril, R. Halogenated Graphenes: Rapidly Growing Family of Graphene Derivatives. *ACS Nano* **2013**, *7*, 6434–6464.

(36) Jiang, X.; Nisar, J.; Pathak, B.; Zhao, J.; Ahuja, R. Graphene Oxide as a Chemically Tunable 2-D Material for Visible-light Photocatalyst Applications. *Journal of Catalysis* **2013**, *299*, 204 – 209.

(37) Yan, J.-A.; Xian, L.; Chou, M. Y. Structural and Electronic Properties of Oxidized Graphene. *Phys. Rev. Lett.* **2009**, *103*, 086802.

(38) Yan, J.-A.; Chou, M. Y. Oxidation Functional Groups on Graphene: Structural and Electronic Properties. *Phys. Rev. B* **2010**, *82*, 125403.

(39) Guilhon, I.; Bechstedt, F.; Botti, S.; Marques, M.; Teles, L. K. Thermodynamic, Electronic, and Optical Properties of Graphene Oxide: A statistical ab Initio Approach. *Phys. Rev. B* **2017**, *95*, 245427.

(40) Sher, A.; van Schilfgaarde, M.; Chen, A.-B.; Chen, W. Quasichemical approximation in binary alloys. *Phys. Rev. B* **1987**, *36*, 4279–4295.

(41) Teles, L. K.; Furthmüller, J.; Scolfaro, L. M. R.; Leite, J. R.; Bechstedt, F. First-principles Calculations of the Thermodynamic and Structural Properties of Strained $In_xGa_{1-x}N$ and $Al_xGa_{1-x}N$ Alloys. *Phys. Rev. B* **2000**, *62*, 2475–2485.

(42) Freitas, F. L.; Furthmüller, J.; Bechstedt, F.; Marques, M.; Teles, L. K. Influence of the Composition Fluctuations and Decomposition on the Tunable Direct Gap and Oscillator Strength of Ge1-xSnx Alloys. *Applied Physics Letters* **2016**, *108*.

(43) Marques, M.; Teles, L. K.; Ferreira, L. G.; Scolfaro, L. M. R.; Furthmüller, J.; Bechstedt, F. Statistical Model Applied to $A_xB_yC_{1-x-y}D$ Quaternary Alloys: Bond Lengths and Energy Gaps of $Al_xGa_yIn_{1-x-y}X$ (X = As, P, or N) Systems. *Phys. Rev. B* **2006**, *73*, 235205.

(44) Kresse, G.; Furthmüller, J. Efficiency of ab-Initio Total Energy Calculations for Metals and Semiconductors Using a Plane-wave Basis Set. *Comput. Mater. Sci.* **1996**, *6*, 15.

(45) Kresse, G.; Hafner, J. Ab Initio Molecular Dynamics for Liquid Metals. *Phys. Rev. B* **1993**, *47*, R558.

(46) Perdew, J. P.; Burke, K.; Ernzerhof, M. Generalized Gradient Approximation Made Simple. *Phys. Rev. Lett.* **1996**, *77*, 3865–3868.

(47) Perdew, J. P.; Burke, K.; Ernzerhof, M. Generalized Gradient Approximation Made Simple [Phys. Rev. Lett. 77, 3865 (1996)]. *Phys. Rev. Lett.* **1997**, *78*, 1396–1396.

(48) Blöchl, P. E. Projector Augmented-wave Method. *Phys. Rev. B* **1994**, *50*, 17953–17979.

(49) Kresse, G.; Joubert, D. From ultrasoft Pseudopotentials to the Projector Augmented-wave Method. *Phys. Rev. B* **1999**, *59*, 1758–1775.

(50) Monkhorst, H. J.; Pack, J. D. Special Points for Brillouin-zone Integrations. *Phys. Rev. B* **1976**, *13*, 5188–5192.

(51) Ferreira, L. G.; Marques, M.; Teles, L. K. Approximation to Density Functional Theory for the Calculation of Band Gaps of Semiconductors. *Phys. Rev. B* **2008**, *78*, 125116.

(52) Pela, R. R.; Marques, M.; Teles, L. K. Comparing LDA-1/2, HSE03, HSE06 and G0W0 Approaches for Band Gap Calculations of Alloys. *Journal of Physics: Condensed Matter* **2015**, *27*, 505502.

(53) Adolph, B.; Gavrilenko, V. I.; Tenelsen, K.; Bechstedt, F.; Del Sole, R. Nonlocality and Many-body Effects in the Optical Properties of Semiconductors. *Phys. Rev. B* **1996**, *53*, 9797–9808.

(54) Gajdoš, M.; Hummer, K.; Kresse, G.; Furthmüller, J.; Bechstedt, F. Linear Optical Properties in the Projector-Augmented Wave Methodology. *Phys. Rev. B* **2006**, *73*, 045112.

(55) Matthes, L.; Pulci, O.; Bechstedt, F. Massive Dirac Quasiparticles in the Optical Absorbance of Graphene, Silicene, Germanene, and Tinene. *Journal of Physics: Condensed Matter* **2013**, *25*, 395305.

(56) Bechstedt, F. *Many-body Approach to Electronic Excitations*; Springer-Verlag Berlin Heidelberg, 2015.

(57) Yang, L.; Deslippe, J.; Park, C.-H.; Cohen, M. L.; Louie, S. G. Excitonic Effects on the Optical Response of Graphene and Bilayer Graphene. *Phys. Rev. Lett.* **2009**, *103*, 186802.

(58) Wirtz, L.; Marini, A.; Rubio, A. Excitons in Boron Nitride Nanotubes: Dimensionality Effects. *Phys. Rev. Lett.* **2006**, *96*, 126104.

(59) Marcano, D. C.; Kosynkin, D. V.; Berlin, J. M.; Sinitskii, A.; Sun, Z.; Slesarev, A.; Alemany, L. B.; Lu, W.; Tour, J. M. Improved Synthesis of Graphene Oxide. *ACS Nano* **2010**, *4*, 4806–4814.

(60) Jung, I.; Field, D. A.; Clark, N. J.; Zhu, Y.; Yang, D.; Piner, R. D.; Stankovich, S.; Dikin, D. A.; Geisler, H.; Ventrice, C. A. et al. Reduction Kinetics of Graphene Oxide Determined by Electrical Transport Measurements and Temperature Programmed Desorption. *The Journal of Physical Chemistry C* **2009**, *113*, 18480–18486.

(61) Eda, G.; Chhowalla, M. Chemically Derived Graphene Oxide: Towards Large-Area Thin-Film Electronics and Optoelectronics. *Advanced Materials* **2010**, *22*, 2392–2415.

(62) Zhou, S.; Bongiorno, A. Origin of the Chemical and Kinetic Stability of Graphene Oxide. *Scientific Reports* **2013**, *3*, 2484.

(63) Lerf, A.; He, H.; Forster, M.; Klinowski, J. Structure of Graphite Oxide Revisited. *The Journal of Physical Chemistry B* **1998**, *102*, 4477–4482.

(64) Nelder, J. A.; Mead, R. A Simplex Method for Function Minimization. *The Computer Journal* **1965**, *7*, 308–313.

Graphical TOC Entry